PROCEEDINGS OF SPIE
SPIE—The International Society for Optical Engineering

Smart Structures and Materials 1999

Mathematics and Control in Smart Structures

Vasundara V. Varadan
Chair/Editor

1–4 March 1999
Newport Beach, California

Sponsored by
SPIE—The International Society for Optical Engineering

Cosponsored by
SEM—Society for Experimental Mechanics
ASME—American Society of Mechanical Engineers
BFGoodrich Aerospace
DARPA—Defence Advanced Research Projects Agency
U.S. Army Research Office

Cooperating Organizations
Air Force Research Laboratory
The Ceramic Society of Japan
Intelligent Materials Forum (Japan)

Published by
SPIE—The International Society for Optical Engineering

SPIE
P
PROCEEDINGS SERIES

Volume 3667

Please use the following format to cite material from this book:
Author(s), "Title of paper," in *Smart Structures and Materials 1999: Mathematics and Control in Smart Structures*, Vasundara V. Varadan, Editor, Proceedings of SPIE Vol. 3667, page numbers (1999).

ISSN 0277-786X
ISBN 0-8194-3141-9

Published by
SPIE—The International Society for Optical Engineering
P.O. Box 10, Bellingham, Washington 98227-0010 USA
Telephone 360/676-3290 (Pacific Time) • Fax 360/647-1445

Printed in the United States of America.

Contents

Modeling dynamics of shape memory alloys via computer algebra

Melnik, Roderick, Roberts, Anthony, Thomas, Kerryn

Roderick V. N. Melnik, Anthony J. Roberts, Kerryn A. Thomas, "Modeling dynamics of shape memory alloys via computer algebra," Proc. SPIE 3667, Smart Structures and Materials 1999: Mathematics and Control in Smart Structures, (4 June 1999); doi: 10.1117/12.350084

Event: 1999 Symposium on Smart Structures and Materials, 1999, Newport Beach, CA, United States

Modelling dynamics of shape-memory-alloys via computer algebra

R.V.N. Melnik*[a], A.J. Roberts[a], K.A. Thomas[a]

[a]Department of Mathematics and Computing,
University of Southern Queensland, QLD 4350, Australia

ABSTRACT

In this paper we present results on numerical studies of the martensitic-austenitic phase transition mechanism in a large shape-memory-alloy rod. Three groups of experiments are reported. They include results on stress- and temperature-induced phase transformations as well as the analysis of the hysteresis phenomenon. All computational experiments are presented for Cu-based structures.

Keywords: Shape memory alloys, phase transition, hysteresis, computer algebra

1. INTRODUCTION

The dynamics of martensitic-austenitic transformations has been investigated experimentally in a wide range of materials, in particular in metallic alloys such as `NiTi`, `CuZnAl`, `CuZnGa`, `CuZn`, `NiAl`, `CuAlNi`, and `AgCd`. Subject to appropriate thermomechanical conditions, these dynamics often exhibit a hysteretic behaviour accompanied by shape-memory effects. For example, if an unstressed shape-memory-alloy wire has been stretched at low temperature, it can be returned to its initial condition upon heating. Upon cooling it can be again returned to its stretched form. In other words, the materials under consideration can be "imprinted" with a shape that they "remember". Not surprisingly these effects have a wide variety of applications ranging from heat engines and different types of actuators to robotics, oceanographic and aerospace industries.

Over recent years, the interest in modelling the dynamics of shape-memory-alloys has been dramatically increased. This includes experimental,[1] theoretical,[2–4] and computational works.[5–8] Current and emerging applications of shape memory alloys require a deeper understanding of structural phase transitions in solids and provide new challenging problems in applied mathematics.

Many smart materials display a strong dependence of load deformation upon temperature. Therefore, in order to adequately model the dynamics of these materials it is important to account for the coupling of stresses, deformation gradients and displacements to the thermal field. Such a coupling is critical in the description of many phenomena that are becoming increasingly important in a wide range of applications of smart materials and structures. The strong nonlinear coupling between thermal and mechanical fields provides an important key to a better understanding of hysteresis-type phenomena. Since these phenomena and the associated shape-memory effects are very difficult to control experimentally, the tools of mathematical modelling and computational experiment play an increasing role in the investigation of thermally and mechanically induced hysteresis in viscoelastic and pseudoplastic materials.

Our main focus in this paper is the adequate description of thermomechanical behaviour of a large shape-memory-alloy rod in the martensitic-austenitic phase transition. Since the description of the mechanism of this transition requires nonconvex free energy functions, this leads to serious mathematical modelling difficulties even in low-dimensional cases.

This paper is a development of our earlier paper,[8] where we derived the two mathematical models used here. In this paper we present three groups of experiments. In the first group of experiments we investigate the mechanical control of phase transitions in shape-memory-alloys. While in Ref. 8 we were interested in phase transitions activated by distributed loading, in this paper we are interested in the dynamics of shape-memory alloys when phase transitions are activated by applied stresses at the body boundary. In the second group of experiments we investigate thermally

*Correspondence: Email: melnik@usq.edu.au; WWW: http://www.sci.usq.edu.au/staff/melnik/;
Telephone: +61 7 46312632; Fax: +61 7 46311775

Part of the SPIE Conference on Mathematics and Control
in Smart Structures • Newport Beach, California • March 1999
SPIE Vol. 3667 • 0277-786X/99/$10.00

induced phase transitions and demonstrate the combined effect of distributed heating and boundary stresses on the development of phase transformations. Finally, we present computational results on and the analysis of hysteresis phenomena for different types of thermomechanical conditions.

We organised the rest of this paper as follows.

- Section 2 gives an overview of the mathematical models used in this paper.
- In Section 3 we provide the reader with the main ideas of our numerical approximations.
- The main part of the paper is Section 4, where we report computational results from the investigation of martensitic-austenitic phase transitions and thermally induced hystereses.
- Finally, in Section 5 we discuss future directions of the presented work.

2. MATHEMATICAL MODELS FOR SHAPE-MEMORY-ALLOY DYNAMICS

The starting point of our present deliberation is this system derived in Ref. 8:

$$\begin{cases} C_v\left[\dfrac{\partial\theta}{\partial t}+\tau_0\dfrac{\partial^2\theta}{\partial t^2}\right]-k_1\left[\theta\dfrac{\partial u}{\partial x}\dfrac{\partial^2 u}{\partial t\partial x}+\tau_0\dfrac{\partial}{\partial t}\left(\theta\dfrac{\partial u}{\partial x}\dfrac{\partial^2 u}{\partial t\partial x}\right)\right]-\mu\left[\left(\dfrac{\partial^2 u}{\partial t\partial x}\right)^2+\right. \\ \left.\tau_0\dfrac{\partial}{\partial t}\left(\dfrac{\partial^2 u}{\partial t\partial x}\right)^2\right]-\nu\left[\dfrac{\partial\theta}{\partial t}\dfrac{\partial^2 u}{\partial t\partial x}+\tau_0\dfrac{\partial}{\partial t}\left(\dfrac{\partial\theta}{\partial t}\dfrac{\partial^2 u}{\partial t\partial x}\right)\right]-\dfrac{\partial}{\partial x}\left(k\dfrac{\partial\theta}{\partial x}\right)=G\,, \\ \rho\dfrac{\partial^2 u}{\partial t^2}-\dfrac{\partial}{\partial x}\left[k_1\dfrac{\partial u}{\partial x}(\theta-\theta_1)-k_2\left(\dfrac{\partial u}{\partial x}\right)^3+k_3\left(\dfrac{\partial u}{\partial x}\right)^5\right]-\mu\dfrac{\partial^3 u}{\partial x^2\partial t}-\nu\dfrac{\partial^2\theta}{\partial x\partial t}=F\,, \end{cases} \tag{1}$$

where u is the displacement field, θ is the temperature field, τ_0 is the thermal relaxation time, k is the thermal conductivity of the material, C_v is the specific heat constant of the material, μ and ν are material-specific coefficients that characterise the dependency of the stress on the rate of the deformation gradient and temperature respectively, ρ is the density of the material, θ_1 is a positive constant that characterises a critical temperature of the material, and k_i, $i=1,2,3$ are material-specific constants that characterise the material's free energy. The right-hand side parts of system (1), F and G, represent the distributed mechanical and thermal loadings of the body.

System (1) is completed by appropriate initial and boundary conditions and has to be solved with respect to (u,θ) in the spatial-temporal region $Q=\{(x,t): 0\le x\le L,\quad 0\le t\le T_f\}$, where L is the length of the structure and T_f is the required time of observation. The initial conditions for the model (1) are taken in the following form

$$u(x,0)=u^0(x)\,,\quad v(x,0)=\frac{\partial u}{\partial t}(x,0)=u^1(x)\,,\quad \theta(x,0)=\theta^0(x)\,,\quad \frac{\partial\theta}{\partial t}(x,0)=\theta^1(x)\,, \tag{2}$$

with specified functions u^0, u^1, θ^0, θ^1. Boundary conditions are problem-specific.[8] In all experiments reported in this paper mechanical boundary conditions are either specified stress or specified displacement:

$$s(0,t)=s_1(t),\quad s(L,t)=s_2(t),\quad \text{or}\quad u(0,t)=u_1(t),\quad u(L,t)=u_2(t); \tag{3}$$

thermal boundary conditions are those of specified heat flux

$$\frac{\partial\theta}{\partial x}(0,t)=\bar\theta_1(t),\quad \frac{\partial\theta}{\partial x}(L,t)=\bar\theta_2(t), \tag{4}$$

where functions $s_i(t)$ (or $u_i(t)$) and $\bar\theta_i(t)$, $i=1,2$ are given.

2.1. The free energy function as a coupling mechanism between mechanical and thermal fields

Temperature plays a critical role in the dynamics of shape-memory-alloys. Under different thermal conditions such materials can exhibit qualitatively different behaviour. For example, at low temperature it is reasonable to expect that shape-memory-alloy materials exhibit *ferroelastic behaviour*. At intermediate temperature they may behave like a *pseudoelastic* material, while at high temperature they behave similar to *elastic* materials.[9] From the mathematical point of view, such a wide range of qualitatively different behaviours is adequately described only if the thermal and mechanical fields are considered together. This coupling is determined by the free energy function. A "slight" change in this function (such as the account for [or omitting of] the viscous or coupled stresses, thermal memory terms, etc[2]) may require completely different mathematical arguments in the analysis of the well-posedness of the model and in the construction of numerical schemes for its solution.

The coupling of thermal and mechanical fields is a key component of the models we deal with in this paper. The description of phase transformations with the model (1)–(4) is based on a non-convex free energy function, which leads to a non-monotone load-deformation curve.[10] This idea, often attributed to van der Waals, was further developed theoretically by Landau and in the context of shape-memory-alloys was pioneered by Falk.[9] The model (1)–(4) incorporates the Helmholtz free energy in the Landau-Devonshire form. In a number of experiments we have also used a modified model (1)–(4) with the Landau-Devonshire-Ginzburg form for the free energy function which assumes the dependency of the free energy on a change of the curvature ϵ_x of the metallic lattice. The form of this dependency determines the coupled stress $\zeta = \zeta(\epsilon_x)$, an extra term in the free energy function, that typically takes the smoothing role of the viscous stress and simplifies the analysis of the mathematical model. The definition of this term varies in the literature with the most common taken to be a quadratic dependency $\gamma/2\epsilon_x^2$, known as the Ginzburg term (γ is the Ginzburg coefficient). This term leads to the appearance of an additional term, γu_{xxxx}, in the first equation of system (1). As we noted in Ref. 8, with reported values of the Ginzburg coefficient ($\gamma \sim 10^{-10} - 10^{-12}$) this term showed little influence on the dynamics of shape-memory alloys in the group of experiments we performed.

2.2. Low-Dimensional Modelling of Shape-Memory-Alloy Dynamics

The properties of shape-memory alloys may strongly depend on chemical composition and on the processing of the material. This often leads to difficulties in comparing different physical experiments. From the mathematical modelling point of view, these difficulties may show themselves in the choice of the free energy function, especially in the higher dimensional case. Indeed, using the analogy with the Landau theory one needs to determine at least 32 material parameters in order to describe thermomechanical behaviour of shape-memory-alloys in 3D.[11,8]

Therefore, some *physically justified assumptions* may be very useful in the mathematical modelling of shape memory alloys. Using such assumptions one can reduce the number of required parameters for Cu-based shape memory alloys to 10. These parameters for $Cu_{14}Al_3Ni_{83}$ (see Ref. 11) have been used in the the construction of a low dimensional model for shape-memory-alloy dynamics in our recent paper.[8] Using the computer algebra package REDUCE such a model has been derived from the 3D Falk-Konopka model[11] for modelling a shape-memory-alloy slab that has a very large extent in the x-direction compared to its thickness ($2b$) in the y-direction ($-b < y < b$). We have assumed that the essential dynamical behaviour of the slab can be determined by a subset of all possible modes. This is a key idea of a quite general methodology arising from centre manifold theory.[12,13]

The model has been constructed with respect to the amplitudes of the critical modes, U_i, V_i ($i = 1, 2$) and Θ' under the assumption that there exists a low-dimensional invariant (slow) manifold upon which these amplitudes evolve slowly. These amplitudes have been chosen as y-averages of u_i, $i = 1, 2$ (displacements in x- and y- directions respectively), v_i, $i = 1, 2$ (velocities in x- and y- directions respectively) and $\theta' = \theta - \theta_0$ with θ_0 taken $300°\ K$. The

model for the longitudinal unforced dynamics of $Cu_{14}Al_3Ni_{83}$ shape-memory-alloy slab has the following form:

$$\begin{cases} \rho\dfrac{\partial V_1}{\partial t} &= 2.97\text{e}6\,U_{1xx} + 8.03\text{e}5\,b^2U_{1xxxx} \\ &\quad + \partial_x\left[(922\,\Theta' - 0.0145\Theta'^2)U_{1x} - (4.28\text{e}9 - 1.31\text{e}7\,\Theta')U_{1x}{}^3 + 7.12\text{e}11\,U_{1x}{}^5\right. \\ &\quad \left. + (2820 - 8.80\,\Theta')b^2V_{1x}{}^2U_{1x} + 1.24\,b^4V_{1x}{}^4U_{1x} - 5.42\text{e}4\,b^2V_{1x}{}^2U_{1x}{}^3\right], \\ \rho\dfrac{\partial V_2}{\partial t} &= -9.91\text{e}5\,b^2U_{2xxxx}\,, \\ C_v\dfrac{\partial\Theta'}{\partial t} &= \kappa\Theta'_{xx} + (2.77\text{e}5 + 914\,\Theta' - 9.25\,\Theta'^2)U_{1x}V_{1x} \\ &\quad + (3.94\text{e}9 + 1.26\text{e}7\,\Theta')V_{1x}U_{1x}{}^3 - (57.3 + 0.0117\,\Theta')b^2V_{1x}{}^3U_{1x} \\ &\quad + 1.68\text{e}12\,V_{1x}U_{1x}{}^5 - 1.58\text{e}6\,b^2V_{1x}{}^3U_{1x}{}^3 - 0.0203\,b^4V_{1x}{}^5U_{1x} \\ &\quad + 1.63\text{e}4\,b^2U_{1xx}V_{1xx} + 9.22\text{e}4\,b^2U_{2xx}V_{2xx} + \partial_x^2\left[-8151\,b^2U_{1x}V_{1x}\right]. \end{cases} \tag{5}$$

Some features of this model are similar to model (1). For example, in the second line of the first equation recognise the temperature dependent stress-strain relation of the shape memory alloy. The model (5) is exact up to the eighth order with respect to the norm $\|\mathbf{U}_x\| + \|\mathbf{V}_x\|$ and the fourth order with respect to two other small parameters chosen in our expansion, ∂_x and $\|\Theta'\|$. Displacements and velocities on the slow manifold are approximately determined using the solution of system (5) as follows (see details in Ref. 8)

$$u_1 \approx U_1 - YbU_{2x} + 0.15(3\,Y^2 - 1)b^2U_{1xx}\,, \tag{6}$$

$$u_2 \approx U_2 - (0.9 - 3.05\text{e-}5\,\Theta')YbU_{1x} + 0.15(3\,Y^2 - 1)b^2U_{2xx} - 141\,YbU_{1x}{}^3 + 1.00\text{e-}4\,(3Y - Y^3)b^3V_{1x}{}^2U_{1x}\,, \tag{7}$$

$$\theta \approx 300 + \Theta' - 2.43\text{e}6\,(3Y - Y^3)b^3\,(V_{1x}U_{2xx} + U_{1x}V_{2xx}) - 25.1(7 - 30\,Y^2 + 15\,Y^4)V_{1x}{}^3U_{1x}\,, \tag{8}$$

where $Y = y/b$ is the scaled transverse coordinate. Unfortunately, as stated in Ref. 11 there has been few experiments on martensitic elastic moduli of shape memory alloys. Perhaps, one of the most widely cited materials is $Cu_{14}Al_3Ni_{83}$ (see Ref. 11). At the time of writing of this paper, we are not aware of parameters for this material for the 1D model. This fact makes it difficult to compare results obtained with low-dimensional and one-dimensional models such as (5)–(8) and (1)–(4). At present, we are using the available parameters for $Au_{23}Cu_{30}Zn_{47}$ (see Ref. 8).

Computer algebra provides a powerful tool in the analysis of shape-memory-alloy dynamics. Indeed, using computer algebra, the model (5)–(8) can be modified to take into account mechanical and/or thermal forcing as well as higher order terms. Currently model (5)–(8) is under our scrutiny.

3. NUMERICAL APPROXIMATIONS

The system (1) is a strongly nonlinear system of partial differential equations that couples hyperbolic and parabolic modes of the dynamics in a unified whole. In the general case, the coupling pattern between thermal and mechanical fields is difficult to analyse. However, if we simplify the system by assuming $\tau_0 = \mu = \nu = 0$, it can be seen that the main terms responsible for the coupling phenomenon are

$$k_1\theta\frac{\partial u}{\partial x}\frac{\partial v}{\partial x} \quad \text{and} \quad \frac{\partial}{\partial x}\left(k_1\frac{\partial u}{\partial x}(\theta - \theta_1)\right) \tag{9}$$

in the first and the second equation respectively. As shall be seen in Section 4, these terms provide the basis for the analysis of the phase transition mechanism.

Several numerical procedures have been reported in the literature for the solution of systems of PDEs describing shape-memory-alloy dynamics (see, for example, Ref. 6,14 and references therein). Our approach is different from those previously reported. The main idea of our approach is a transformation of the problem (1)–(4) into a system of differential-algebraic equations with respect to (u, v, θ, s). Then we solve this system using second-order accurate spatial differences on staggered grids. The developed MATLAB code is simple, robust and easy to implement.

Taking into account the above assumptions the transformed system for all computational experiments described in Section 4 has the following form

$$\begin{cases} \dfrac{\partial u}{\partial t} &= v, \\ \rho\dfrac{\partial v}{\partial t} &= \dfrac{\partial s}{\partial x} + F, \\ C_v\dfrac{\partial \theta}{\partial t} &= k\dfrac{\partial^2\theta}{\partial x^2} + k_1\theta\dfrac{\partial u}{\partial x}\dfrac{\partial v}{\partial x} + G, \\ s &= k_1(\theta-\theta_1)\dfrac{\partial u}{\partial x} - k_2\left(\dfrac{\partial u}{\partial x}\right)^3 + k_3\left(\dfrac{\partial u}{\partial x}\right)^5. \end{cases} \tag{10}$$

The term $\dfrac{\partial u}{\partial x} = \epsilon$ in (10) is the linearised strain that plays the role of the order parameter in the Landau theory.

The initial and boundary conditions for this model are problem-specific and will be defined in the next section. All experiments reported here were performed for a $Au_{23}Cu_{30}Zn_{47}$ rod of the length $L = 1$cm. For the $Au_{23}Cu_{30}Zn_{47}$ material all necessary parameters were first specified by Y. Murakami (see ref. in Falk[9]). In the context of system (10) we use (see also Ref. 6,8)

$$k = 1.9\times10^{-2}\text{cmg/(ms}^3\text{K)}, \quad \rho = 11.1\text{g/cm}^3, \quad C_v = 29\text{g/(ms}^2\text{cmK)}, \quad \theta_1 = 208\text{K}\,,$$

$$k_1 = 480\text{g/(ms}^2\text{cmK)}, \quad k_2 = 6\times10^6\text{g/(ms}^2\text{cmK)}, \quad k_3 = 4.5\times10^8\text{g/(ms}^2\text{cmK)}\,.$$

4. COMPUTATIONAL EXPERIMENTS

Due to a wide range of industrial applications and associated challenging applied mathematics problems, the control of phase transitions in shape memory alloys has recently become a topic of considerable interest.[3] In this section we investigate different options for the control of shape memory alloys, including stress-boundary control, distributed heating and their combination. Special attention is given to the computational analysis of hysteresis.

4.1. Stress Induced Phase Transitions

The stress-induced phase transition exhibits a hysteresis, provided that we have thermodynamic barriers to prevent an equilibrium phase transition.[9] In the following two experiments the role of these barriers is played by the boundary stress chosen as the main control variable.

Experiment 1.1. First, in the spirit of Ref. 7, let us consider the following initial conditions

$$u(x,0) = \epsilon_0 x\,, \quad v(x,0) = 0\,, \quad \theta(x,0) = 230\,. \tag{11}$$

Choosing $\epsilon_0 = 0.106051$ the rod is initially in martensitic phase M_+. For the given initial temperature this state is stable and we need to change thermomechanical conditions of the rod to induce a phase transition (for such a low temperature the same is also true for M_- martensitic phases).

We assume no distributed loading (i.e. $F = G = 0$). Instead, for the first 6 ms we load the rod at the boundaries (which are assumed to be thermally insulated) with the compressive load $-7000\sin^3(\pi t/6)\,\text{g/(ms}^3\text{cm)}$. Then, for the next 6 ms we do not apply any force, and for the next 6 ms after that we apply a tensile load $7000\sin^3(\pi t/6)\,\text{g/(ms}^3\text{cm)}$. Therefore, we have the following boundary conditions on $x = 0$ and L:

$$\frac{\partial\theta}{\partial x} = 0\,, \quad s = \begin{cases} -7000\sin^3(\pi t/6), & 0\le t\le 6, \\ 7000\sin^3(\pi t/6), & 12\le t\le 18, \\ 0, & \text{otherwise.} \end{cases} \tag{12}$$

During the initial period, observe the phase transformation $M_+ \to M_-$ in Fig. 1. Then, observe the appearance of two regions with a slight increase/decrease in displacement (upward and downward "humps"). These regions demonstrate *thermomechanical coupling effects* between the two phases in the period when the temperature pattern

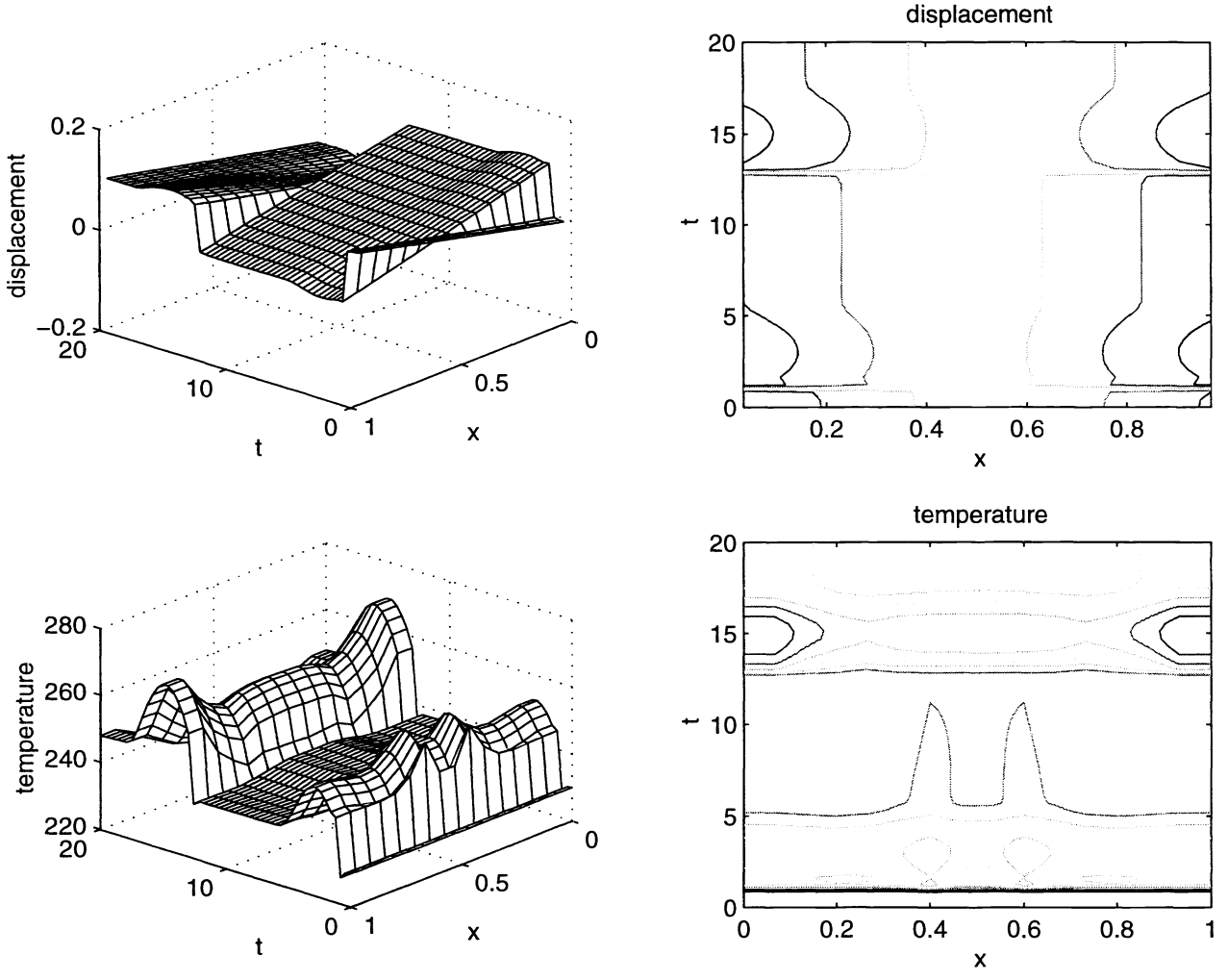

Figure 1. Stress induced phase transition: the tensile load exceeds the yield limit.

changes (see temperature plots in Fig. 1). After a while, one observes that these regions vanish and we have only the M_- phase which is in stable equilibrium. Finally, observe a reverse phase transformation $M_- \to M_+$ (due to the tensile load) according to a pattern which is analogous to that described above.

The behaviour of this type is typical for ferro-elastic materials. When subjected to low initial temperatures, shape memory alloys do not produce an intermediate austenite phase under the above thermomechanical conditions.

Experiment 1.2. In the previous example we saw that after the transformation $M_+ \to M_-$ takes place, the reverse transformation $M_- \to M^+$ is possible under fairly high tensile loading exceeding the yield limit. If the last condition is not satisfied, the rod would remain in the M_- phase. This is demonstrated by the next experiment, where the tensile loading was set 10 times lower than in the previous example:

$$s = \begin{cases} -7000 \sin^3(\pi t/6), & 0 \le t \le 6, \\ 700 \sin^3(\pi t/6), & 12 \le t \le 18, \\ 0, & \text{otherwise.} \end{cases} \tag{13}$$

All other conditions remained the same as in Experiment 1.1. The effect of thermomechanical coupling (after the transition $M_+ \to M_-$) is observed only for a short period of time. It results in small perturbations visible on Fig. 2 as the regions with two "humps". After that the rod returns to the M_- stable equilibrium.

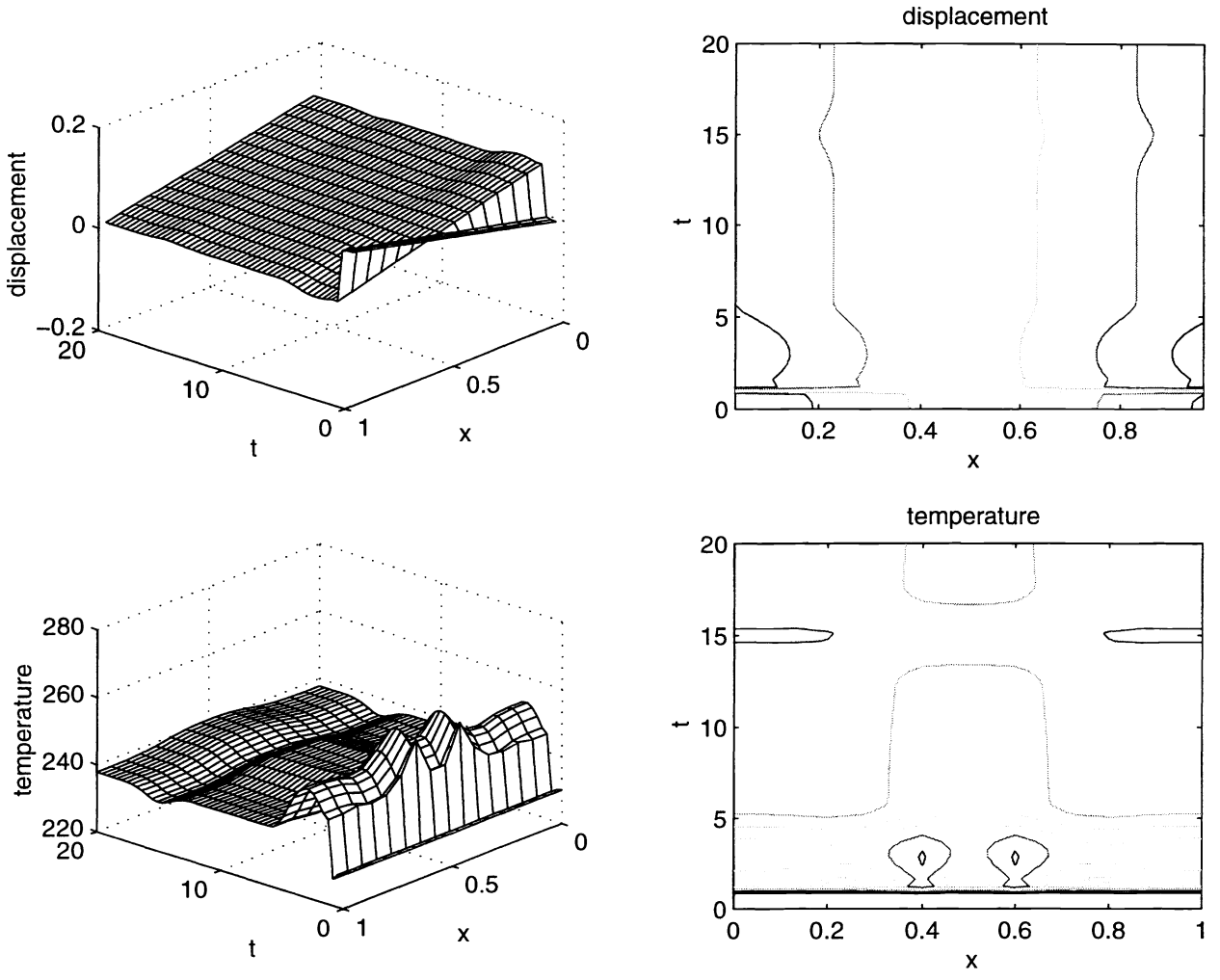

Figure 2. Absence of thermodynamic barriers to prevent an equilibrium phase transition: the tensile load is less than the yield limit.

The situation will not qualitatively change if we keep a constant load (say, $s = 100$) for all the times when the compressive/tensile load at the boundary is absent, i.e. when

$$s = \begin{cases} -7000\sin^3(\pi t/6), & 0 \le t \le 6, \\ 700\sin^3(\pi t/6), & 12 \le t \le 18, \\ 100, & \text{otherwise.} \end{cases} \tag{14}$$

The almost-linear behaviour of displacements on the second stage of this experiment suggests that the rod exhibits elastic properties under the given thermomechanical conditions.

With spatial and temporal steps $0.6\bar{6}$ cm and 9.26×10^{-4} ms respectively, experiments 1.1 and 1.2 take on average 10–11 minutes to complete on a Digital Alpha 255 station (300 MHz).

4.2. Temperature Induced Phase Transitions

The purely mechanical control of phase transitions discussed in Section 4.1 may not be efficient. In the next experiment we show how to control this process by temperature. More precisely, we explore the range of temperature

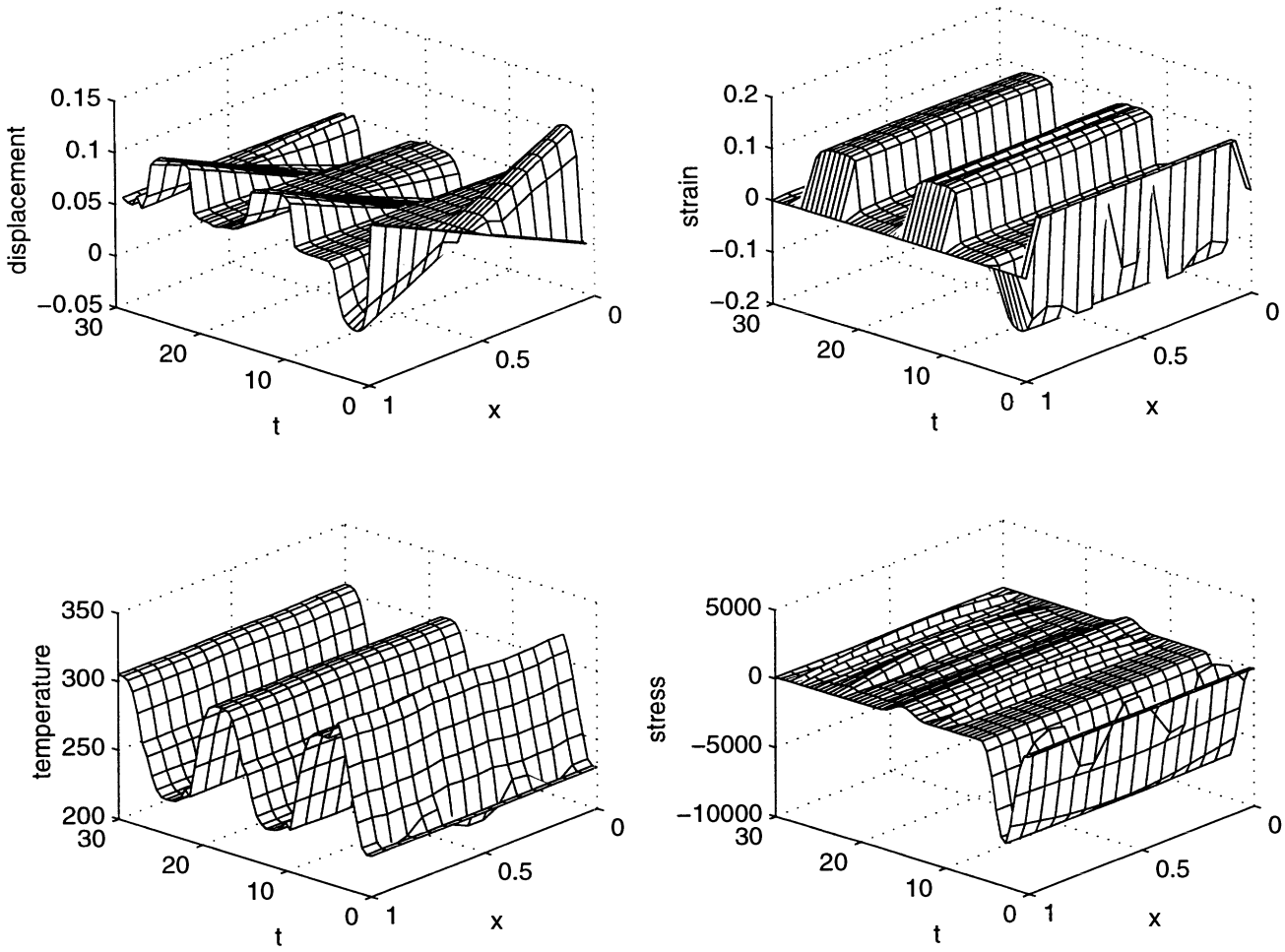

Figure 3. Temperature controls thermodynamic barriers allowing phase transitions even if the tensile load is less than the yield limit.

for which on cooling the formation of martensite starts; and conversely, the range of temperature, for which on heating, the formation of austenite starts.

The driving force for this type of transition is the difference between the free energies of both phases. We control this difference by controlling the distributed heating/cooling pattern.

Experiment 2.1. Consider our last experiment where we were unable to produce a phase transition with the given loading pattern. Let us keep the stress on the boundary such that (14) is satisfied and all other conditions, except for the distributed thermal loading, remain the same as in Experiment 1.2. The distributed heating/cooling used is

$$G = 375 \sin^3(\pi t/6)\ \mathrm{g/(ms^3 cm)}\,. \tag{15}$$

Then, after the initial switch $M_+ \to M_-$ (due to insufficiently low initial temperature), we observe phase transitions (see Fig. 3)

$$M_- \to A, \quad \text{then} \quad A \to M_+, \quad M_+ \to A \quad \text{etc.} \tag{16}$$

The hyperbolic features of this transitions are demonstrated by the stress plot presented on Fig. 3.

This experiment shows that in those cases when the mechanical load alone is not sufficient to induce the phase transition in the rod, we can effectively use distributed heating/cooling to control the phase transition process.

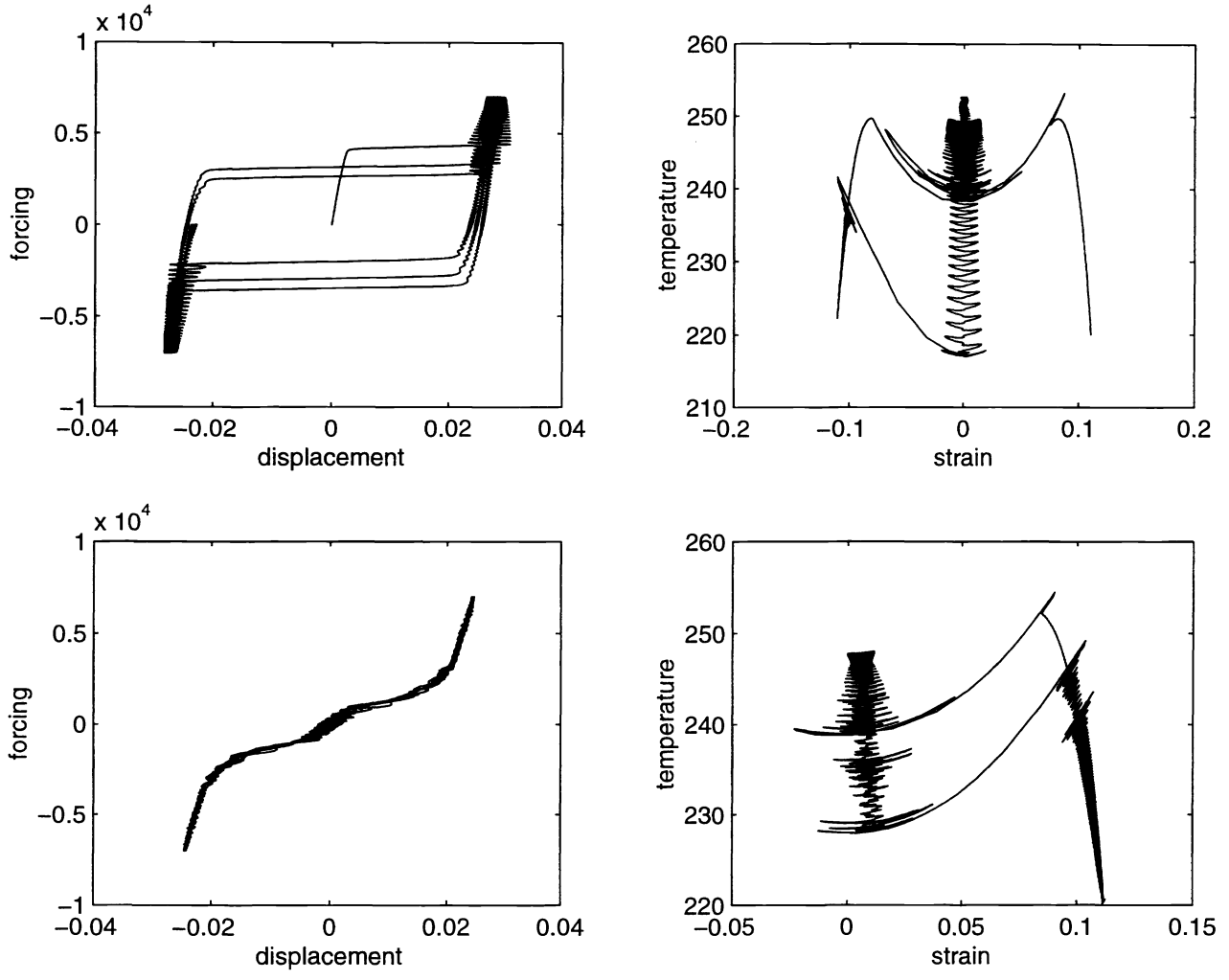

Figure 4. Mechanically and thermally induced hystereses.

4.3. Hysteresis Analysis

The non-convexity and the non-linear thermal dependency of the free energy function, used in the derivation of mathematical models such as (1)–(4) and (5)–(8), play key roles in the understanding of hysteresis-type phenomena. Indeed, in the general case these characteristics imply non-monotone stress-stress relationships (or load-deformation diagrams) which depend on the temperature change in a complicated nonlinear manner. We explore such situations below.

Experiment 3.1. Again consider the case of mechanical loading in the low-temperature regime. However, in contrast to Experiment 1.1, we start with two M_+ and one M_- martensites, so that the initial conditions for this experiment are

$$\theta^0 = 220\,, \quad u^0 = \begin{cases} 0.11869x, & 0 \le x \le 0.25, \\ 0.11869(0.5-x), & 0.25 \le x \le 0.75, \\ 0.11869(x-1), & 0.75 \le x \le 1, \end{cases} \qquad v^0 \equiv u^1 = 0. \tag{17}$$

Another difference from previously considered examples is the pinned mechanical boundary conditions

$$u = 0\,, \quad \frac{\partial \theta}{\partial x} = 0\,. \tag{18}$$

In the absence of thermal loading ($G = 0$) we assume the following time-dependent distributed mechanical loading

$$F = 7000 \sin^3\left(\frac{\pi t}{2}\right) \text{ g/(ms}^3\text{cm)}\,. \tag{19}$$

Since under these thermomechanical conditions shape-memory-alloys behave like a ferroelastic material, one may expect a hysteresis loop to be observed.[15,5] This phenomenon is clearly demonstrated by the upper left plot on Fig. 4.

Experiment 3.2. Under intermediate-temperature conditions, shape-memory alloys behave like pseudoelastic materials. In this case, in spite of the difference in loading/unloading stress-strain curves, the mechanical loading does not lead to a residual strain.[9]

In our next experiment we start from the martensitic state M_+ given by the following initial conditions:

$$u^0 = 0.11869x\,, \quad v^0 = 0\,, \quad \theta^0 = 270\,. \tag{20}$$

The thermal and mechanical distributed loading are the same as in Experiment 3.1, but we also apply stress at the thermally insulated boundaries according to the following rule

$$s = \begin{cases} -1000 \sin^3(\pi t/6), & 0 \le t \le 6, \\ 0, & \text{otherwise}, \end{cases} \qquad \frac{\partial \theta}{\partial x} = 0. \tag{21}$$

The given temperature is on the border of the "pseudoelastic" range and the two symmetric loops, that are typical for these thermomechanical conditions, are very small (see the lower-left plot on Fig. 4). Further increase in temperature leads to the complete disappearance of hysteresis since in this case shape-memory-alloys start to behave like elastic materials.

The concluding two experiments are aimed at the description of hystereses in thermally-induced phase transformations.

Experiment 3.3. Two symmetric martensites are taken as the initial state for the next experiment, namely

$$u^0 = \begin{cases} 0.11869x, & 0 \le x \le 0.5, \\ 0.11869(1-x), & 0.5 \le x \le 1, \end{cases} \qquad v^0 = 0\,, \quad \theta^0 = 220\,. \tag{22}$$

In this experiment we assume constant distributed loading of $F = 500\text{g/(ms}^3\text{cm)}$ and the following thermal distributed loading

$$G = \frac{375}{2}\pi \sin^3\left(\frac{\pi t}{6}\right) \text{g/(ms}^3\text{cm)}\,. \tag{23}$$

On the boundary we assume that

$$u = 0\,, \quad \frac{\partial \theta}{\partial x} = 0\,. \tag{24}$$

The temperature-strain plot, presented on the right-upper plot of Fig. 4, demonstrates temperature-induced transformations between austenite and martensites. See that these transformations are approximately symmetric with respect to the sign of strain.

Experiment 3.4. Finally, we assume no mechanical distributed loading ($F = 0$). We start from an M_+ martensitic state defined by the following initial conditions:

$$u^0 = 0.11869x\,, \quad v^0 = 0\,, \quad \theta^0 = 220\,. \tag{25}$$

Boundary conditions are those of stress-free, insulated ends:

$$s = 0\,, \quad \frac{\partial \theta}{\partial x} = 0\,, \tag{26}$$

while the distributed thermal loading is assumed to follow the same pattern as in Experiment 3.3. The lower-right plot of Fig. 4 gives the temperature-strain curve of the phase transformation between M_+ and A states.

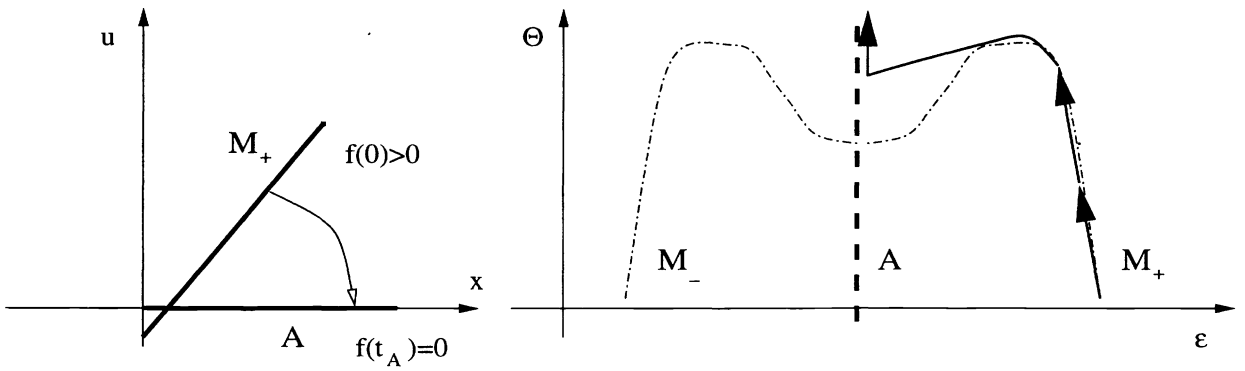

Figure 5. Schematic representations of thermally induced hystereses.

With spatial and temporal steps 0.0625 cm and 6.67×10^{-4} ms respectively, the last 4 experiments take on average 33–36 minutes to complete on a Digital Alpha 255 station.

The overall shape of the temperature-strain curves in Experiment 3.3 and 3.4 are explained using a simple approximate analysis that follows. Let us assume that the strain varies in time but is more-or-less uniform over the rod: $\dfrac{\partial u}{\partial x} \approx \varsigma f(t)$ with a certain constant coefficient ς (see Fig. 5 for a schematic representations of the transformation $M_+ \to A$). Then, integrating this relationship (assuming the mean displacement to be zero) we get

$$u = \varsigma x f(t) \quad \text{and, hence,} \quad v = \varsigma x \frac{\partial f}{\partial t}\,. \tag{27}$$

After differentiating (27) we have that $\dfrac{\partial v}{\partial x} = \varsigma \dfrac{\partial f}{\partial t}$.

On the other hand, in the absence of diffusion ($k = 0$) when $\tau_0 = 0$ and $\mu = \nu = 0$, the thermal equation of system (1) is

$$\frac{\partial \theta}{\partial t} = k_c \theta \frac{\partial u}{\partial x}\frac{\partial v}{\partial x}\,, \quad \text{where} \quad k_c = k_1/C_v\,. \tag{28}$$

Using the above representations for $\dfrac{\partial u}{\partial x}$ and $\dfrac{\partial v}{\partial x}$ in terms of the function f, from (28) we get that

$$\frac{1}{\theta}\frac{\partial \theta}{\partial t} = k_c \varsigma^2 f \frac{\partial f}{\partial t}\,. \tag{29}$$

Hence, taking into account that $f = \dfrac{1}{\varsigma}\dfrac{\partial u}{\partial x}$, an approximation to the strain-temperature relationship is derived directly from (29) as

$$\ln \frac{\theta}{\theta_c} = \frac{k_c}{2}\varsigma^2 f^2 \quad \text{or} \quad \ln \frac{\theta}{\theta_c} = \frac{k_c}{2}\left(\frac{\partial u}{\partial x}\right)^2\,, \tag{30}$$

where θ_c is a constant. The last relationship confirms the parabolic shape of the temperature-strain curves in the transitions from martensites to austenites as depicted on the right-hand side plots of Fig. 4.

5. FUTURE DIRECTIONS

Physical experiments suggest the possible existence of non-equilibrium states inside of hysteresis loops.[15] Therefore, the geometry of hysteresis loops as a function of temperature requires further investigations. Mathematical modelling and computational experiments in such investigations provide a very useful and powerful tool. For a deeper understanding of hysteresis phenomenon in shape-memory-alloys further computational experiments are needed. An important direction of these experiments is the comparison of results obtained with different mathematical models such as (1)–(4) and (5)–(8).

Another aspect of future work follows from the evidence that the width of hysteresis may often be determined by an additional term which is responsible for the interfacial energy and when this term vanishes the phase transition may occur reversibly.[10] Mathematical models that are derived using free energy functions that incorporate interfacial energy contributions and take into account the influence of mechanical and thermal dissipations (such as the latent heat) may prove to be helpful.

Strictly speaking the models presented in this paper are applicable only for single crystals. A much more complex task is to describe the dynamic of composite heterogeneous materials. Such materials often arise in structural engineering when dealing, for example, with polymer based composites, in biomechanics, and in food industries. Some composites such as fiber-reinforced polymers, are formed as a mixture of elastic and viscoelastic materials.[16] Mathematical modelling of the dynamics of such materials, including their thermoviscoelastic contacts, present a challenge for future work.

ACKNOWLEDGMENTS

This work was supported by USQ-PTRP Grant 179452 and by Australian Research Council Grant 179406.

REFERENCES

1. H. Benzaoui, C. Lexcellent, N. Chaillet, B. Lang, and A. Bourjault, "Experimental study and modelling of a tini shape memory alloy wire actuator," *Journal of Intelligent Material Systems and Structures* **8**, pp. 619–629, 1997.
2. J. Sprekels, "Global existence for thermomechanical processes with nonconvex free energies of ginzburg-landau form," *Journal of Mathematical Analysis and Applications* **141**, pp. 333–348, 1989.
3. N. Bubner, J. Sokolowski, and J. Sprekels, "Optimal boundary control problems for shape memory alloys under state constraints for stress and temperature," *Numer. Funct. Anal. and Optimiz.* **19**(5&6), pp. 489–498, 1998.
4. R. S. Anderssen, I. G. Gotz, and K.-H. Hoffmann, "The global behavior of elastoplastic and viscoelastic materials with hysteresis-type state equations," *SIAM J. Appl. Math.* **58**(2), pp. 703–723, 1998.
5. O. Klein, "Stability and uniqueness results for a numerical approximation of the thermomechanical phase transitions in shape memory alloys," *Advances in Mathematical Sciences and Applications (Tokyo)* **5**(1), pp. 91–116, 1995.
6. M. Niezgodka and J. Sprekels, "Convergent numerical approximations of the thermomechanical phase transitions in shape memory alloys," *Numer. Math.* **58**, pp. 759–778, 1991.
7. H. Alt, K.-H. Hoffmann, M. Niezgodka, and J. Sprekels, "A numerical study of structural phase transitions in shape memory alloys," Tech. Rep. 90, Department of Mathematics, University of Augsburg, 1985.
8. R. V. N. Melnik and A. J. Roberts, "Approximate models of dynamic thermoviscoelasticity describing shape-memory-alloy phase transitions," in *New Methods in Applied and Computational Mathematics (NEMACOM'98)*, D. Stewart and S. Oliviera, eds., *Proc. of the Centre for Mathematics and its Applications* (to appear; see `http://www.sci.usq.edu.au/cgi-bin/wp/research/workingpapers`) , 1998.
9. F. Falk, "Model free energy, mechanics, and thermomechanics of shape memory alloys," *Acta Metallurgica* **28**, pp. 1773–1780, 1980.
10. I. Muller and H. Xu, "On the pseudo-elastic hysteresis," *Acta Metall. Mater.* **39**(3), pp. 263–271, 1991.
11. F. Falk and P. Konopka, "Three-dimensional landau theory describing the martensitic phase transformation of shape-memory alloys," *J. Phys.: Condens. Matter.* **2**, pp. 61–77, 1990.
12. J. Carr, *Applications of Centre Manifold Theory*, Springer, Berlin, 1981.
13. S. M. Cox and A. J. Roberts, "Centre manifolds of forced dynamical systems," *J. Austral. Math. Soc. Ser. B* **32**, pp. 401–436, 1991.
14. K.-H. Hoffmann and J. Zou, "Finite element approximations of landau-ginzburg's equation model for structural phase transitions in shape memory alloys," M^2AN **29**(6), pp. 629–655, 1995.
15. M. Bornert and I. Muller, "Temperature dependence of hysteresis in pseudoelasticity," in *Free Boundary Value Problems*, K.-H. Hoffmann and J. Sprekels, eds., pp. 27–35, Birkhauser, 1990.
16. H. I. Ene, M. L. Mascarenhas, and J. S. J. Paulin, "Fading memory effects in elastic-viscoelastic composites," M^2AN **31**(7), pp. 927–952, 1997.